Biophysical Journal, Volume *117*

Supplemental Information

Dynamics of Mechanosensitive Nascent Adhesion Formation

Laurent MacKay and Anmar Khadra

Manuscript submitted to **Biophysical** *Journal*
Article

Supporting Material

Laurent MacKay[1] and Anmar Khadra[1,*]

[1]Department of Physiology, McGill University, Montreal, Quebec, Canada
[*]Correspondence: anmar.khadra@mcgill.ca

MODEL FRAMEWORK

The primary process which results in the formation of a nascent adhesion (NA) is the clustering of integrins (1). It has been suggested that very small non-specific clusters of integrin spontaneously form even in the absence of ligand binding; however, their size and spatial distributions were inconsistent with that of NAs formed in the presence of ligand binding (2). Generally speaking, in the presence of ligand, NAs were about twice as large (compared to those generated in the absence of ligand), exhibited high variability in their integrin content, and yet had a relatively restricted distribution in their size (2). This suggests that (i) there is an intrinsic clustering mechanism for integrins, (ii) ligand binding enhances this clustering mechanism to form NAs, and (iii) the area of the cluster is not directly proportional to its integrin content (i.e., there is a nonlinear relation between NA-area and the number of integrins forming it). Interestingly, it has been observed that integrins exhibit reduced diffusivity within adhesions (defined experimentally by the area underneath an adaptor protein plaque), by at least a factor of three (3). This decrease was found to be dependent on interactions with adaptor proteins through the cytoplasmic domain of integrins, suggesting that membrane-proximal adaptor proteins may exert a drag force on integrins (3). Integrins also undergo extended periods of immobilization which further decreases their lateral mobility. The frequency of long-lived immobilization is enhanced inside adhesions and has been found to be dependent on integrin's interaction with both extracellular ligands and adaptor proteins (3, 4). Thus we propose that the NA-area, as defined by the adaptor protein plaque, provides an environment within which integrin lateral mobility is decreased due to both a reduced diffusion coefficient and increased likelihood of binding to extracellular ligand.

Reduced integrin lateral mobility, due to their interactions with the adaptor protein and extracellular ligands plaque, may explain aggregation of integrins into micron-scale clusters. This, however, does not explain the presence of the adhesion plaque. Firstly, its was previously argued, from a theoretical perspective, that adhesion plaques must be self-assembling structures in order to explain the stress-induced growth of adhesions (5). Meanwhile, the adaptor protein talin and its interaction with integrins have been repeatedly found to be required for the formation of NAs (2, 6, 7). These results suggest, that the self-assembly of adhesion plaques requires both integrin and adaptor proteins to be capable of forming complexes with one another. Furthermore, increased extracellular ligand density (and thus integrin density inside the adhesion) has been shown to increase the residence time of the adaptor protein FAK inside the adhesion plaque (8). Additionally, the diffusivity of the adaptor protein paxillin shows significant heterogeneity in its value inside a single adhesion plaque, suggesting that paxillin may exist in more than one association state within the adhesion (9–11). We propose that adaptor proteins form membrane-proximal aggregates around a seed of a small number of integrins, and that subsequent retention of integrins inside the adhesion area (as discussed above) allows for growth of the adhesion plaque due to the decreased mobility of adaptor proteins. This decreased mobility manifests itself in the model as a decrease in the off-rate of adaptor proteins in the presence of integrins. The precise nature of the mechanism which reduces the off-rate will depend on the specific adaptor protein in question. In the model developed herein, we generically describe it as a reversible tethering to the membrane by integrin.

Together, these effects constitute a mechanism for the self-aggregation of cytoplasmic adaptor proteins and integrins, a phenomenon we refer to hereafter as co-aggregation. More specifically, we propose that (i) integrin lateral mobility is modulated locally by the presence of membrane-proximal adaptor proteins, and (ii) adaptor proteins are effectively tethered to the membrane by integrins. In this manner, the presence of a protein of one type increases the probability that a protein of the other type will be present in close proximity. This positive feedback between the two types of proteins would allow them to serve as templates for one another in the formation of membrane-proximal aggregates of adaptor protein (i.e., an adhesion plaque). We incorporate this mechanism into a mathematical model that satisfies the following assumptions (see Fig. 1A):

1. Adaptor proteins are modeled as either being in a well-mixed cytosolic bulk phase or in a spatially confined region $\Omega(t) \in \mathbb{R}^2$ which delimits the adhesion. Their density ρ inside NAs (i.e., the domain Ω) is assumed to be uniform. Furthermore, we impose the conservation of matter by assuming that the adaptor protein content of a NA is drawn from a

finite reservoir of N_P adaptor proteins, and therefore the number of cytosolic adaptor proteins N_{cyto} is given by

$$N_{cyto} = N_P - \rho A, \tag{S1}$$

where $A := \|\Omega\|$ is the surface area of the adhesion plaque. This means that, as NAs grow very large, they will deplete the cytoplasmic pool of adaptor proteins until an equilibrium between their growth and shrinkage rates is reached. When adaptor proteins are in the adhesion plaque, they can either be associated with the rest of the adaptor protein scaffold or they may be bound to an integrin receptor where they become reversibly tethered to the membrane. We assume that individual adaptor proteins leave the adhesion at a rate k_{off} and $(1-\delta)\,k_{off}$, where $\delta \in (0,1)$, when they are untethered and tethered to integrin, respectively. This difference in off-rate in the presence of integrins is what leads to the aggregation of adaptor proteins around integrins.

2. We model integrins as 2-dimensional (2D) Brownian particles that diffuse freely outside the adhesion, and exhibit reduced mobility within the adhesion domain Ω. This reduced mobility is implemented through two biophysical mechanisms. In the first, we assume that the diffusion coefficient of integrins is lower when they are underneath the adhesion plaque, i.e.,

$$D(x) = \begin{cases} D_{in} & x \in \Omega \\ D_{out} & \text{otherwise} \end{cases}, \tag{S2}$$

where $D_{in} \leq D_{out}$ are the diffusion coefficients inside and outside the adhesion domain Ω, respectively (3). In the second, we make the simplifying assumption that only the adhesion environment provides the necessary ingredients for the long-lived immobilization of integrin, which we attribute to ligand binding (3). Therefore, we assume that integrins inside Ω may bind to an extracellular ligand and become reversibly immobilized with a binding affinity K_{bind}.

Spatial Assumptions

We consider a periodic array of adhesions on a square lattice with an inter-adhesion spacing h. This simplifying assumption of periodicity allows us to study the problem on a small $h \times h$ square patch of membrane that is assumed to receive no net flux of matter from adjacent patches (see Fig. 1B) because they are all in equilibrium. We further consider that the $h \times h$ square patch contains N_I integrins and sits under the adhesion plaque consisting of N_P adaptor proteins. Integrins are assumed to diffuse in a 2-dimensional plane (i.e., the membrane), and a circular aggregation of adaptor proteins centered at the origin with an area A that delimits the region defining the adhesion plaque (i.e., $\Omega = \left\{(x,y) : \pi\left(x^2+y^2\right) \leq A\right\}$).

Integrin Reaction-Diffusion Model

In order for the force transmission through an adhesion to the ECM to be effective, its integrins must bind to their extracellular ligands. When bound to their ligand, integrins exhibit a diverse range of mobilities (3, 12, 13). Generally, we can expect the integrins to have a reduced mobility upon binding to ligand. We consider the extreme case of complete immobilization in order to understand what can be expected at most from the ligand binding process. Within an adhesion, only a certain proportion of integrins are bound to ligand (3, 4, 14). We denote the total number of integrins inside the adhesion area by N_{in}, while L_{in} and M_{in} denote the number of liganded and mobile integrins, respectively (i.e., $N_{in} = L_{in} + M_{in}$). If we assume that ligand-binding induced immobilization happens only within the adhesion, then the dynamics of M_{in} is given by

$$\dot{L}_{in}(t) = k_{unbind}\left(K_{bind} M_{in} - L_{in}\right) := R_{bind},$$

where k_{unbind} is the unbinding rate of an integrin, and K_{bind} is its binding affinity, given by

$$K_{bind} = \frac{k_{bind}}{k_{unbind}},$$

with k_{bind} denoting the first order binding rate of a single integrin (assuming fixed extracellular ligand density). In order to account for variations in the density of extracellular ligand, denoted $\left[\text{Ligand}\right]$, we use the expression

$$k_{bind} = \overline{k}_{bind}\left[\text{Ligand}\right], \tag{S3}$$

where $\overline{k}_{bind}$ is a the second order binding rate.

An unbound integrin is assumed to diffuse freely in the cellular membrane. We use the Fokker-Planck (FP) diffusion equation to describe the spatiotemporal evolution of the unbound integrin density $I(x)$. Such a model has a local flux $j(x)$, given by

$$j(x) = \nabla \left(D(x) I(x) \right), \tag{S4}$$

where ∇ is the gradient operator and $D(x)$ is the diffusion coefficient. In situations with inhomogeneous diffusion coefficient, such as Eq. S2, this FP flux equation is more applicable than the more widely used Fick's law (15). We are interested in the time-invariant (equilibrium) behaviour of the adhesion; we therefore assume zero-flux boundary conditions on the outer edge of the membrane patch. This corresponds to finding a solution where the flux is zero everywhere. For a piecewise constant diffusion coefficient, such a solution is expected to be piecewise constant at equilibrium, given by

$$I(x) = \begin{cases} I_{in} & x \in \Omega \\ I_{out} & \text{otherwise,} \end{cases}$$

where I_{in} (I_{out}) is the density of unbound integrins inside (outside) the adhesion (16). However, the discontinuity in Eq. S2 leads to to a singular flux at the interface between the adhesion plaque boundary and the rest of the membrane, given by

$$j_0 = (D_{out} I_{out} - D_{in} I_{in}) \hat{r},$$

where $\hat{r}$ is the radial unit vector (17). As time tends towards infinity, diffusion smooths out all concentration gradients such that the non-singular portion of the flux in Eq. S4 becomes zero irrespective of the integrin densities in and out of the adhesion. Therefore, near equilibrium, we take the total flux of free integrins into the adhesion due to diffusion to be the integral along the interface of the singular component of the flux

$$J_{in} = \int_0^{2\pi} j_0 \cdot \hat{r} r d\theta = (D_{out} I_{out} - D_{in} I_{in}) 2\pi r,$$

where r is the radius of the adhesion. We note that $I_{in} = M_{in}/A$ and thus, by imposing conservation of matter, we eliminate the variable I_{out} to obtain the relation $I_{out} = (N_I - N_{in})/(h^2 - A)$. Finally, the rate of change of unbound integrins inside the adhesion is given by the difference between the integrated diffusive flux and the binding reaction rate, i.e.,

$$\dot{M}_{in} = J_{in} - R_{bind}. \tag{S5}$$

We have assumed in the derivation of Eq. (S5) that diffusion reaches its equilibrium within NAs. Although it is often assumed that NAs are far from equilibrium due to their short stability period (18–21), recent evidence suggests that conditions preventing NA-disassembly produces integrin clusters with very similar properties (in terms of number and size) to those that do disassemble (2). This indicates that NAs come very close to their equilibrium before disassembling, and motivates the treatment of integrin dynamics near the equilibrium of the diffusion process in this study.

Adhesion Plaque Adsorption Model

To capture the kinetics of adaptor protein aggregation into a membrane-proximal plaque, we adapt the "Bulk-on/Bulk-off" model of adsorption (22), where adhesions are assumed to be able to grow (shrink) from any point in its interior by addition (subtraction) of adaptor proteins that are incorporated into the adhesion with a uniform density ρ. Adaptor proteins are assumed to be added to an adhesion at a rate

$$\gamma(A) = A k_{on}^0 P_{out}, \tag{S6}$$

where $P_{out} = \frac{N_{cyto}}{h^2}$ is the density (per unit area) of free adaptor proteins. Furthermore, we consider that integrins inside the adhesion stabilize the adhesion plaque leading to less adaptor proteins leaving the adhesion per unit time. In the model, this is implemented by assuming that adaptor proteins can exist in two states within the adhesion, one which is reversibly tethered to the membrane by integrins and the other loosely associated with adjacent adaptor proteins. Adaptor proteins can leave the adhesion plaque with a rate k_{off} and $(1-\delta) k_{off}$ for the untethered and tethered states, respectively. Assuming that fast kinetics govern the association of integrins and adaptor proteins within the adhesion, we prescribe a phenomenological Hill-function expression for the off-rate of an adaptor protein, given by

$$\kappa\left(N_{in}/A\right) = k_{off} \left((1-\delta) + \delta \frac{b^n}{b^n + \left(N_{in}/A\right)^n} \right), \tag{S7}$$

where N_{in}/A is the total integrin density in the adhesion, k_{off} is the maximal observed degradation rate of the adhesion, δ is the magnitude of the co-aggregation between integrins and adaptor proteins (a value of 0 indicating no co-aggregation while a value of 1 indicating full co-aggregation), n is the degree of cooperativity between integrins for the tethering of adaptor proteins ($n = 1$ indicates no cooperativity while $n > 1$ indicates positive cooperativity), and b is the integrin density needed to tether 50% of adaptor proteins. Based on this, we obtain the following dynamic equation for adhesion area

$$\frac{dA}{dt} = \frac{1}{\rho}\left(\gamma(A) - A\rho\kappa(I_{in})\right) = A\left[\frac{k_{on}^0 P_{out}}{\rho} - \kappa\left(N_{in}/A\right)\right].$$

Geometric Constraints

The complete set of equations governing NA dynamics are given by Eqs. 1a-1c (see main text). The equilibria of the system lie at the intersection of its nullsurfaces. The plane $A = 0$ is one of the A-nullsurfaces, while

$$L_{in}^* = K_{bind} M_{in}^* \tag{S8}$$

is the L_{in}-nullsurface, and

$$M_{in}^* = \frac{A^* C_I K_{in} h^2}{A^*\beta + h^2} \tag{S9}$$

is the M_{in}-nullsurface, where $K_{in} = D_{out}/D_{in}$ and $\beta = \left(K_{in}(1 + K_{bind}) - 1\right)$. At the intersection of these nullsurfaces, we have the steady state $\mathbf{Z} = (A, M_{in}, L_{in}) = (0, 0, 0)$, representing the unclustered configuration of adhesion proteins (with both adaptor proteins and integrin receptors uniformly distributed in space). The second A-nullsurface (see Eq. 2) forms with the other nullsurfaces a steady state where adhesion proteins are co-aggregated into a dense cluster. The conditions which cause the system to switch between the unclustered and the clustered steady states are analyzed in the main text. Nonetheless, from Eq. S9, we can see that $N_{in} \to \infty$ as $C_I \to \infty$ provided that $A \neq 0$. In this limit, integrins have their maximum effect on the aggregation of adaptor proteins, and thus the clustered steady state will reach some maximum area A^∞. According to the second term in Eq. 1a, this maximum area is given by

$$A^\infty := h^2\left(\frac{C_P}{\rho} - \frac{1-\delta}{K_{on}}\right), \tag{S10}$$

where $K_{on} = k_{on}^0/k_{off}$. The first term in Eq. (S10) is the maximal fractional area the adhesion plaque can attain if all adaptor proteins become stuck to the membrane, while the second term is a correction factor that accounts for the finite binding affinity of adaptor proteins being absorbed into the plaque. This indicates that A^∞ depends linearly on the adaptor protein density, and remains finite regardless of the integrin density. It is important to consider the geometric assumptions of our model, in order to ensure that its predictions are physically meaningful. By letting $\phi = [(C_P/\rho) - ((1-\delta)/K_{on})]$, we obtain $A^\infty = h^2\phi$. For a circular adhesion lying strictly within a square lattice cell, we must have $\phi \in \left[0, \pi/4\right)$ in order for the results of our model to remain biophysically relevant.

Generally, if we were to formulate this model for some other lattice with a unit cell area A_{max} (e.g., $A_{max} = h^2$ for the square lattice), we can adapt all our results by replacing h^2 with the particular value of A_{max}. In such a case, the upper bound on ϕ will depend on the geometry of the lattice and the adhesion; however, in general, we will always have $\phi < 1$ as a maximum upper bound. For $\phi \geq 1$, our circular adhesions will take up more area than is available for the given lattice, and thus the membrane will be saturated with adhesion plaque on the length scale h. Because ϕ is independent of the lattice geometry, we interpret this upper bound as being set by the biophysical and chemical properties of the proteins involved rather than an artifact of the periodic lattice assumption.

Transcritical Bifurcation

The switch between the unclustered $\mathbf{Z} = (0, 0, 0)$ and clustered $\mathbf{S}^* = \left(A^*, M_{in}^*, L_{in}^*\right)$ steady states occurs at a transcritical bifurcation point. In what follows, we analyze the stability properties of this steady state. As discussed in the main text, for simplicity we focus on the case $n = 1$. Under these conditions, the Jacobian matrix of the system evaluated at the unclustered steady state has three eigenvalues, two of which are strictly negative and one that can change its sign, given by

$$\lambda_1 = k_{on}^0\left(\phi - \frac{b\delta}{bK_{on} + \hat{C}_I}\right).$$

Hence, the unclustered steady state is unstable if $\lambda_1 > 0$. A switch in the sign of λ_1 can occur when certain parameters of the model cross a threshold. For the intracellular densities C_I and C_P, these thresholds are given by

$$C_I > C_I^{\ddagger} := \frac{b\left(\delta - \phi K_{on}\right)}{\phi K_{on} K_{in}\left(1 + K_{bind}\right)} \tag{S11}$$

and

$$C_P > C_P^{\ddagger} := \frac{\rho\left(b + K_{in}\left(1 + K_{bind}\right) C_I\left(1 - \delta\right)\right)}{K_{on}\left(b + K_{in}\left(1 + K_{bind}\right) C_I\right)} \geq 0, \tag{S12}$$

respectively. Moreover, the threshold for the binding affinity K_{bind} is given by

$$K_{bind} > K_{bind}^{\ddagger} := \frac{b\delta - \phi K_{on}\left(b + C_I K_{in}\right)}{\phi C_I K_{in} K_{on}}$$

which, according to Eq. S3, can produce the following threshold for ligand concentration

$$\left[\text{Ligand}\right] > \left[\text{Ligand}\right]^{\ddagger} := \frac{k_{unbind}}{\overline{k}_{bind}} \frac{b\delta - \phi K_{on}\left(b + C_I K_{in}\right)}{\phi C_I K_{in} K_{on}}. \tag{S13}$$

Once the system passes through the transcritical bifurcation, the model gives birth to the clustered steady state $\mathbf{S}^*$ representing a stable adhesion plaque with area A^* that contains $N_{in}^* = M_{in}^* + L_{in}^*$ integrins.

Integrin Mechanosensitivity

Integrin mechanosensitivity is thought to arise from mechanically-induced conformational changes. It has been suggested that the mechanical extension and separation of the extracellular legs of integrin receptors results in a long-lived bound state (23, 24). We incorporate these ideas into our model as a force-dependent ensemble average lifetime $\left\langle \tau\left(f\right)\right\rangle$, where f is the force applied on the integrin. This is modeled using the two-pathway model of bond-dissociation (25), given by

$$\left\langle \tau\left(f\right)\right\rangle = \tau_0\left(de^{\hat{f}(c+d)} + c\right) \frac{1}{ce^{fd} + de^{\hat{f}(c+d)}e^{-cf}}, \tag{S14}$$

where τ_0 is the bond lifetime with zero applied force, $\hat{f}$ is the force which optimizes the bond lifetime, and $c, d > 0$ are coefficients. These coefficients are determined numerically by first setting

$$d = \frac{c\hat{\tau}}{\tau_0 e^{c\hat{f}} - \hat{\tau}} + \frac{1}{\hat{f}} \times W\left(-\frac{c\hat{f}\tau_0 e^{-\frac{c\hat{f}\hat{\tau}}{\tau_0 e^{c\hat{f}} - \hat{\tau}}}}{\tau_0 e^{c\hat{f}} - \hat{\tau}}\right),$$

where $\hat{\tau} = \left\langle \tau\left(\hat{f}\right)\right\rangle$ is the optimal bond lifetime and $W\left(\cdot\right)$ is the W-Lambert function, followed by varying c in such a way that $\left\langle \tau\left(60\,\text{pN}\right)\right\rangle \approx 0.1$ s (see Fig. S1 for profile and Parameter Estimation for numerical values). Finally, this give the numerical expression

$$\left\langle \tau\left(f\right)\right\rangle = \frac{1}{0.666667exp(-0.0876215F) + 6.60165 \times 10^{-8}\exp(0.313789f)} \tag{S15}$$

In order to incorporate the mechanosensitive properties of integrins into our binding model, we set the integrin unbinding rate k_{unbind} to be the reciprocal of $\left\langle \tau\left(f\right)\right\rangle$, the ensemble bond lifetime. This means that

$$K_{bind} = k_{bind}\left\langle \tau\left(f\right)\right\rangle, \tag{S16}$$

(i.e., all bound integrins are assumed to bear an equal load). The numerical value of f is determined by assuming that the NA experiences a fixed stress (force per unit area), given by

$$\sigma = \frac{fL_{in}}{A}. \tag{S17}$$

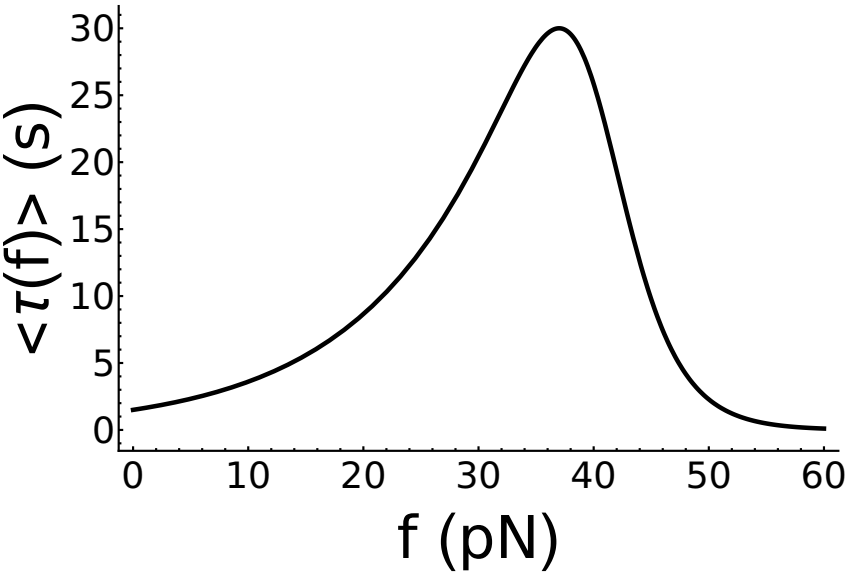

Figure S1: Integrin-ligand bond lifetime, $\langle \tau(f) \rangle$, as a function of f, the applied force per integrin. The biphasic profile resembles that obtained for catch bonds between integrin and fibronectin (26).

Stochastic Simulations

We note that the integrin flux described by Eq. S5 is only valid for small perturbations around the steady state as it neglects the effects of concentration gradients. In order to more accurately capture the full integrin dynamics specified in Eq. S4 far from equilibrium, we re-formulate our model as a discrete system, where we use a master equation approach to describe the aggregation of adaptor proteins at the adhesion plaque and the reversible binding of integrins within the adhesion region. Furthermore, to account for the diffusion of integrins along the membrane, we use a Brownian dynamics approach where each integrin is given a position $\vec{x}(t)$ that evolves in time according to a Brownian motion with local diffusivity given by Eq. S2, and use the Euler-Maruyama update scheme to obtain the time-dependent positions of integrins (27). By denoting the number of adaptor proteins in the adhesion plaque by i, we obtain the following total number of integrins $\nu(t)$ inside a NA of area $A = i/\rho$

$$\nu(t) = \sum_{k=1}^{N_I} \begin{cases} 1 & \text{if } \pi \vec{x}_k(t) \cdot \vec{x}_k(t) \leq i/\rho \\ 0 & \text{otherwise,} \end{cases}$$

where $\vec{x}_j(t)$ is the position of the j^{th} integrin at time t. Setting p_i to be the probability of having a NA with i adaptor proteins, we conclude that the aggregation of adaptor proteins at the adhesion plaque obeys a master equation, given by

$$\rho \dot{p}_i(t) = \left(g_{i-1} p_{i-1} + s_{i+1}(\nu(t)) p_{i+1}\right) - \left(g_i + s_i(\nu(t))\right) p_i, \tag{S18}$$

where g_i (s_i) is the growth (shrinkage) reaction-rate, defined by $g_i = \gamma(i/\rho)$ and $s_i(\nu) = i\kappa(\rho\nu/i)$, respectively. Letting ℓ_j be the probability of having j bound integrins inside the adhesion, we obtain the following master equation for binding kinetics of integrin

$$\dot{\ell}_j(t) = k_{bind}\left(\nu(t) - (j-1)\right)\ell_{j-1} + (j+1)k_{unbind}\ell_{j+1} - \left(k_{bind}\left(\nu(t) - j\right) + jk_{unbind}\right)\ell_j. \tag{S19}$$

When integrins become bound, we reversibly set their diffusion coefficient to zero, and set their unbinding rate to $k_{unbind} = \langle \tau(i\sigma/\rho j) \rangle^{-1}$. The time-course of the chemical reactions is realized through a temporal Gillespie algorithm, that allows for efficient stochastic simulations of reactions with time-dependent propensities (28). This is necessary to account for the fact that both reactions have propensities which depend on $\nu(t)$, and that integrins may diffuse into or out of the adhesion independently of the reactions governed by Eqs. S18 or S19.

Parameter Estimation

Model parameter values are inferred, when possible, using algebraic expressions from the model equated to values obtained from experimental measurements. In the main text, we have identified two regions of interest in parameters space, which we

have denoted regions 2 & 3. The assumptions inherent in each region leads to slightly different algebraic expressions for model parameters. We begin by discussing the expressions that the two regions have in common, followed by explaining the distinct approaches used in each region.

Firstly, we introduce the relative enrichment of integrins inside the adhesion E, which has been observed to be in the range of $E \in [2, 12]$ in various physiological conditions (3, 29). Using the conservation of matter for integrins, we obtain the following expression for their density

$$C_I = \frac{I_{in}\left(A_1 + \left(h^2 - A_1\right)/E\right)}{h^2}, \tag{S20}$$

where I_{in} is the density of integrins inside the adhesion, A_1 is the mean area of NA (to be estimated from experimental measurements), and h is the mean inter-adhesion spacing. The parameter h is determined using

$$\bar{N}^*_{in} := \lim_{K_{bind}\to\infty} M^*_{in} + L^*_{in} = C_I h^2$$

which can be combined with Eq. (S20) to yield

$$h = \left(A_1\left(1 - E\right) + E\frac{N_2}{I_{in}}\right)^{1/2}, \tag{S21}$$

where N_2 is the number of integrins in a NA when integrin binding is very strong (also to be determined from experimental measurements). Secondly, an expression for the parameter b can be obtained by solving $I_{in} = N^*_{in}/A^*$, with $N^*_{in} = L^*_{in} + M^*_{in}$, to obtain

$$b = \frac{I_{in}K_{on}\left(-(\beta+1)C_I + \beta\phi I_{in} + I_{in}\right)}{(\beta+1)C_I K_{on} - I_{in}\left(-\beta\delta + \beta\phi K_{on} + K_{on}\right)}, \tag{S22}$$

where the estimation of the parameters K_{on} and K_{in} (implicit in β) must be dealt with differently in the two regions. We may also use the model steady states to derive the expression

$$E = \frac{N^*_{in}/A^*}{\left(N_I - N^*_{in}\right)/\left(h^2 - A^*\right)} = \left(1 + K_{bind}\right)K_{in}$$

which may be rewritten as an expression for the binding affinity, given by

$$K_{bind} = \frac{E}{K_{in}} - 1. \tag{S23}$$

The parameter δ is estimated by considering the ratio of FRAP recovery times of the intermediate and slow fractions of the adaptor protein paxillin and vinculin within focal adhesions (10). This ratio is in the range of 20-80, corresponding to a value of $\delta \in [0.95, 0.99]$. We also estimate the value of the mean density of adaptor proteins prior to adhesion formation, C_P, using the literature value of paxillin concentration $[\text{paxillin}] \approx 2.3\,\mu$M multiplied by an estimate of cell volume $V_{cell} \approx 1000\,\mu\text{m}^3$ to get the total number of paxillin molecules in the cell $N_{pax} \approx 1.38 \times 10^6$ (30). We then use the simple approximation $C_P \approx N_{pax}/A_{cell} = 8050\mu\text{m}^{-2}$, where $A_{cell} \approx 172\,\mu\text{m}^2$ is the estimated cell area determined from analysis of imaging data (2), to obtain $C_P \approx 8050\,\mu\text{m}^{-2}$. Finally, the parameters k_{off} and ρ are chosen in such a way that stochastic simulations of adhesion disassembly/assembly have a timescale and stochasticity comparable to that observed experimentally (19), respectively.

Region 3

From a super-resolution quantification of adhesion size and integrin content (2), we can obtain the following estimates $I_{in} \approx 6600\,\mu\text{m}^{-2}$ and $A_1 \in [7, 9] \times 10^{-3}\,\mu m^2$. The integrin clusters produced by the same study (2), upon exposing cells to Mn^{+2} (which switches integrins into a high-affinity state), can be used to obtain the estimate $N_2 \approx 75$. Using Eq. (S21), with $E \approx 12$ (i.e., by assuming that NAs are among the most enriched in integrins) and $A_1 \approx 8.7 \times 10^{-3}\,\mu m^2$, we obtain $h \approx 0.2\,\mu m$. This estimate is further verified visually by analyzing the spacing between NAs in images (2). Furthermore, region 3 is differentiated from region 2 by the fact that it produces adhesions even in the absence of ligand binding. Experimentally, in the absence of ligand, it was found that small clusters of integrin containing $N_3 \in [4, 19]$ integrins form with an area $A_3 \in [1, 4.4] \times 10^{-3}\mu m^2$ (2). We use these quantifications to aid us in our parameter estimation by setting them equal to appropriate model steady states, i.e., by letting

$$N_3 = \tilde{M}^*_{in} + \tilde{L}^*_{in} \tag{S24}$$

Table S1: Auxiliary parameter values used in the determination of model parameters (see Table S3 for model parameter values).

Symbol	Definition	Estimated Value	Reference(s)
E	Fold-enrichment of integrins within the adhesion	12	(3, 29)
I_{in}	Mean density of integrins within the adhesion	6600 μm^2	(2)
A_1	Mean NA-area	8.7×10^{-3} μm^2	(2)
N_2	Number of integrins inside NAs when Mn^{2+} is added to extracellular medium	75	(2)
$[\text{paxillin}]$	Physiological paxillin concentration	2.3 μM	(30)
V_{cell}	Volume of a mouse embryonic fibroblast (MEF) cell	1000 μm^3	-
A_{cell}	Area of a MEF cell	172 μm^2	(2)
N_3	Number of integrins inside NAs in the absence of extracellular ligands	6	(2)
A_3	Mean NA-area in the absence of extracellular ligands	2.7×10^{-3} μm^2	(2)
$\langle\tau\,(0\,\text{pN})\rangle$	Ensemble average of integrin-ligand bond lifetime in the absence of force	1.5 s	(26)
$\langle\tau(\hat{f})\rangle$	Ensemble average of the optimal integrin-ligand bond lifetime	30 s	(31)
$\hat{f}$	The force that optimizes bond lifetime	37 pN	(26)
$\langle\tau\,(60\,\text{pN})\rangle$	Ensemble average of the integrin-ligand bond at very large forces	0.1 s	(26)

and

$$A_3 = \tilde{A}^*. \tag{S25}$$

These two expressions are then used in conjunction with Eqs. (S20), (S22), and (S23) to yield

$$K_{in} = \frac{N_3\left(\left(A_1(E-1)+A_3\right)I_{in} - EN_2\right)}{A_3\left(N_3-N_2\right)I_{in}} \approx 1.2, \tag{S26}$$

$$K_{on} = \frac{\delta\left(\frac{EN_2}{I_{in}} - A_1(E-1)\right)\left(A_3\left(A_1-A^\infty\right)I_{in} + N_3\left(A^\infty - A_3\right)\right)}{\left(A^\infty-A_1\right)\left(A^\infty-A_3\right)\left(N_3-A_3I_{in}\right)} \approx 0.70, \tag{S27}$$

$$K_{bind} = \frac{\left(A_1-A_3\right)(E-1)N_3I_{in} + EN_2\left(A_3I_{in}-N_3\right)}{N_3\left(EN_2 - \left(A_1(E-1)+A_3\right)I_{in}\right)} \approx 8.8, \tag{S28}$$

and

$$b = \frac{A_3I_{in}\left(A^\infty - A_1\right) + N_3\left(A_3 - A^\infty\right)}{\left(A_1-A_3\right)A_3}, \tag{S29}$$

where we have used $\delta \approx 0.97$, $A_2 \approx 2.7\times10^{-3}$ μm^2, and $N_3 \approx 6$ (b remains to be determined). The parameter A^∞ is determined from data. More specifically, using the *maximum a posteriori* (MAP) estimate of the relation between adhesion area and its integrin content (see dotted line in Fig. 2). This data is fit to the A-nullcline given by Eq. (2) using a nonlinear least squares approach and taking Eq. (S29) into consideration . The values of the fit parameters and their 95% confidence bounds are provided in Table S2. The confidence interval on the quantities b and A_0 are relatively large, indicating that they are not well constrained by the data at hand. Nonetheless, these confidence intervals do not contain zero and only cover one order of magnitude, so we deem them to be acceptable. This completes model parameter estimation in Region 3 necessary to generate quantitative understanding of the model developed in this study.

Region 2

Region 2 ($[\text{Ligand}]^\ddagger > 0$) can be distinguished from region 3 ($[\text{Ligand}]^\ddagger < 0$) by the fact that NAs will not form in the absence of ligand. As discussed in the main text, the transition from region 2 to region 3 may be achieved by decreasing K_{on}. We therefore keep the numerical values of all other parameters determined in region 3 as is, and use a different formalism for

Table S2: Least-squares estimates of model parameters and confidence intervals obtained from a nonlinear least squares fitting of the A-nullcline to data.

Symbol	Least-Squares Estimate	95% Confidence Interval
A^{∞}	$0.0124\,\mu\text{m}^2$	$[0.0118, 0.0129]\ \mu\text{m}^2$
b	$463\,\mu\text{m}^{-2}$	$[68.8, 806]\ \mu\text{m}^{-2}$
A_0	-0.038	$[-.0204, -0.239]\ \mu\text{m}^2$

determining K_{on}. More precisely, we use Eqs. (S13), (S20), and (S21) to obtain

$$K_{on} = \frac{b\delta\left(EN_2 - A_1(E-1)I_{in}\right)^2}{A^{\infty}I_{in}\left(N_2\left(bE + I_{in}K_{in}\left([Ligand]^{\ddagger}\frac{\bar{k}_{bind}}{k_{unbind}} + 1\right)\right) - A_1 b(E-1)I_{in}\right)}, \tag{S30}$$

where we have used previous experimental finding to estimate $\left[\text{Ligand}\right]^{\ddagger} \approx 200\mu m^{-2}$, and the ratio $\bar{k}_{bind}/k_{unbind} = 0.005$ was chosen such that the equilibrium of NA-area $A^* \approx A^{\infty}$ for ligand densities given by $\left[\text{Ligand}\right] \geq 10,000\,\mu\text{m}^{-2}$ (see Fig. 3 in main text) as suggested by the spreading behaviour of cells when cultured on substrates with variable ligand density (32, 33)

Mechanosensitivity of Integrin

The coefficients in Eq. S14 are determined based on atomic force microscopy data on the bond lifetime of integrins (26, 31). More specifically, we have $\left\langle \tau\left(0\,\text{pN}\right)\right\rangle = 1.5$ s, $\langle\tau\rangle$ has a maximum at 37 pN, $\left\langle \tau\left(37\,\text{pN}\right)\right\rangle = 30$ s, and $\left\langle \tau\left(60\,\text{pN}\right)\right\rangle = 0.1$ s. Using these values, the coefficients $d \approx 0.32$ and $c \approx 0.088$ that appear in Eq. (S14) are determined (as discussed before) algebraically and by numerical optimization, respectively.

CONDITIONAL EXPECTATION ANALYSIS

Introduction

In numerous scientific applications, quantitative measurements of a system near a quasi-equilibrium are made and then analyzed. Rather than providing a precise description of a system, we may assume that it can be (at least partially) described by a set of measurements (e.g., a population may be described by the body temperature of its individuals, or a macro-molecular complex may be described by its mass and charge). Let us consider the simple experimental scenario in which measurements of two quantities of interest X and Y are made. These may represent the same quantity in two different conditions or two different quantities in the same condition. If there is a relation between the two measurements X and Y due to the intrinsic interactions of the system under study, one may attempt to derive this relation from experimental data. However, this task is complicated by the presence of stochastic fluctuations, measurement error, heterogeneity between realizations, and large data sets. With this in mind, let us consider a pair of correlated random variables (X, Y) measured simultaneously from a dynamical system near a unique equilibrium $\left(\bar{X}, \bar{Y}\right)$ using a homoscedastic model

$$(X, Y) = \left(\bar{X}, \bar{Y}\right) + (\chi, \gamma)\,,$$

where χ (along with γ) is an independent identically distributed additive noise. If both quantities X and Y have an effect on the dynamics of the physical system being observed, the equilibrium $\bar{Y}$ can be expressed as

$$\bar{Y} = f\left(\bar{X}\right). \tag{S31}$$

Given samples of (X, Y), collected under a variety of experimental conditions, it may not be straight-forward to estimate $f(\cdot)$ if the values of the corresponding $\left(\bar{X}, \bar{Y}\right)$ cannot be readily determined. This situation may arise when studying phenomena at the sub-cellular level, due to high levels of both intracellular and inter-cellular heterogeneity present even when the experimental

Table S3: Model parameter values used in the numerical simulations. Parameter values are obtained either directly from the literature or estimated analytically using model-derived equations as indicated in columns labelled source. Parameter values and sources which are different in region 3 are in parentheses.

Symbol	Definition	Value Region 2 (Region 3)	Source Region 2 (Region 3)
δ	Fractional decrease in adaptor protein off-rate (k_{off}) when tethered by integrin.	0.97	Ref. (10)
b	Integrin density inside adhesion which tethers 50% of adaptor proteins	463 μm^{-2}	Eq. (S29)
C_I	Mean density of integrins in the membrane	1844 μm^{-2}	Eq. (S20) ’
h	Mean distance between adhesions	0.20 μm	Eq. (S21)
K_{in}	D_{out}/D_{in}	1.22	Eq. (S26)
D_{out}	Diffusion coefficient of integrin outside the adhesion	0.28 μm^{2}s^{-1}	Refs. (3, 4)
D_{in}	Diffusion coefficient of integrin inside the adhesion	0.22 μm^{2}s^{-1}	$K_{in} = \frac{D_{out}}{D_{in}}$
K_{on}	Affinity of adaptor protein adsorption reaction in the absence of integrins	0.29 (0.7)	Eq. (S30) (Eq. (S27))
k_{off}	Adaptor protein off-rate in the absence of integrins	1.0 s^{-1}	-
k_{on}^0	Kinetic parameter governing on-rate for adsorption of adaptor proteins into the adhesion plaque††	0.31 s^{-1} (0.73 s^{-1})	$K_{on} = \frac{k_{on}^0}{k_{off}}$
ρ	Density of adaptor proteins in the adhesion plaque	4000 μm^{-2}	-
ϕ	Maximum fractional area of a NA	0.30	Least-Squares
C_P	Basal density of adaptor proteins in the cytosol	8050 μm^{-2}	Ref. (30)
K_{bind}	Binding affinity of single integrins	8.81	Eq. (S28)
k_{bind}	Binding rate of single integrins (= $\overline{k}_{bind}$[Ligand])	2.58 s^{-1}	$k_{bind} = \frac{K_{bind}}{\langle \tau(0\,\mathrm{pN}) \rangle}$

†† In order to obtain an estimate of the first order reaction rate for a bi-molecular adaptor protein binding event, we can use Eq. (S6) with $A = \rho^{-1}$ and $P_{out} = C_P$. This yields binding rate estimates of 0.62 s^{-1} and 1.5 s^{-1} in regions 2 and 3, respectively.

conditions are fixed. In order to circumvent this difficulty, we employ the probability distributions of X and Y instead. Assuming that χ (γ) is independent of $\bar{X}$ ($\bar{Y}$), we can compute the observed probability density of X (Y) as

$$\begin{aligned} P_X &= P_{\bar{X}} * P_{\chi}, \\ P_Y &= P_{\bar{Y}} * P_{\gamma}, \end{aligned}$$

where $*$ denotes the convolution operator. Assuming that f is a monotonic function, the the probability distribution of $\bar{Y}$ is related to that of $\bar{X}$ by the *change of variable equation,* given by

$$P_{\bar{Y}}(f) = P\left(\bar{Y} = y \,|f\right) = \frac{P_{\bar{X}}(x)}{|f'(x)|}, \tag{S32}$$

where f' is the derivative of f and x is the pre-image of y (i.e., $x = f^{-1}(y)$).

Experimentally, one may repeatedly measure both X and Y and approximate the marginal distributions P_X and P_Y by binning data to make the histograms $\mathbf{P_X}$ and $\mathbf{P_Y}$, respectively. In what follows, we will explain a methodology for determining f from these histograms.

Relation to Previous Work

The task of deducing a transformation $f(\cdot)$ from data is central to numerous machine learning techniques. However, these techniques differ in their motivation from the data analysis task we have presented above. For example, in the unsupervised learning methods of density estimation and manifold learning/unfolding the transformation f is used to more efficiently represent data in a so-called representation space, which is useful when dealing with very high dimensional data (34–37). Such methods assume that P_X is unknown and use well known parametric distributions as a prior on X in their inference of f. Such

approaches are inappropriate for our needs as they ignore the data $\mathbf{P_X}$, and thus it is unlikely that the inferred f would satisfy Eq. (S32). Alternatively, Gaussian Process models and Generalized Additive Models have both been used in supervised learning tasks to infer relationships between experimentally measured variables X and Y (38–40). However, these approaches require pairing of the data into coordinates (X, Y), which may not always be possible. On the other hand, our approach requires only knowing the marginal distributions $\mathbf{P_X}$ and $\mathbf{P_Y}$ which may be readily estimated from unpaired (or paired) samples of X and Y. Moreover, a great deal of the algorithmic complexity seen in the literature is motivated by issues which arise in high-dimensions (41), while our data is intrinsically one-dimensional.

Overview of the Algorithm

Given the experimentally determined discrete estimates $\mathbf{P_X}$ and $\mathbf{P_Y}$, we propose decomposing the problem of estimating f into two steps:

1. Finding a maximum a posteriori (MAP) discrete estimates of $P_{\bar{X}}$ and P_χ, which we denote $\hat{\mathbf{P}}_{\bar{\mathbf{X}}}$ and $\hat{\mathbf{P}}_\chi$, respectively. This may can be accomplished using the blind deconvolution algorithm (42). We note that it is also possible to do the same for $P_{\bar{Y}}$ and P_γ, but without the mapping f (or f^{-1}) it is unclear whether these estimates satisfy Eq. (S32).

2. We estimate f and P_γ by solving the minimization problem

$$\begin{cases} \min_{f,P_\gamma} & \mathrm{KL}\left(P_{\bar{Y}}\left(f\right) * P_\gamma \,|P_Y\right) + \lambda \mathrm{BV}\left(P_{\bar{Y}}\left(f\right)\right) \\ \text{subject to} & f' > 0,\ P_\gamma \geq 0\ \left\|P_\gamma\right\| = 1, \left\|\gamma P_\gamma\right\| = 0, \end{cases} \tag{S33}$$

where $\mathrm{KL}\left(p\,|q\right) = \int_{-\infty}^{\infty} p\left(x\right) \log\left(p\left(x\right)/q\left(x\right)\right) dx$ is the Kullback-Leibler Divergence, $P_{\bar{Y}}\left(f\right)$ is given by Eq. (S32), λ is a non-negative parameter, and $\mathrm{BV}\left(u\right) = \left\|u'\left(x\right)\right\|_2$ is a Tikhonov regularization term (43) which limits the irregularity of the estimate $P_{\bar{Y}}$. Here we have formally restricted our optimization to monotonically increasing functions ($f' > 0$), but we may also consider monotonically decreasing functions by substituting in the constraint $f' < 0$.

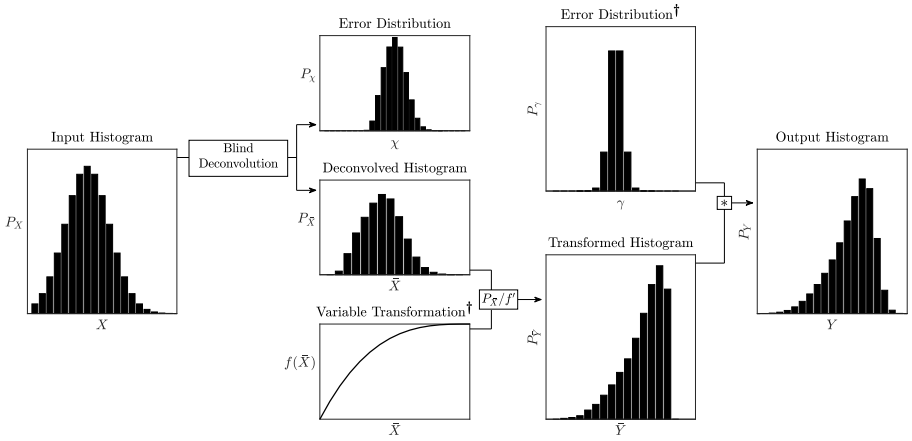

Figure S2: Schematic overview of the computational approach used to estimate P_Y given P_X, $f(\bar{X})$, and P_γ. The quantities that we seek to infer ($f(\bar{X})$ and P_γ) are marked with †.

Parametrization

Generally speaking, Bayesian inference methods, such as Markov Chain Monte Carlo (MCMC) techniques, produce samples of parameters θ, some of which may be used to estimate f. In this section, we detail our approach for reconstructing f from a given set of parameters θ. In the following section, we detail how to compare the experimental data $\mathbf{P_Y}$ to the model prediction $P_Y\left(\theta\right) = P_{\bar{Y}}\left(f\left(x\right)|\theta\right) * P_\gamma\left(\theta\right)$ in order to produce appropriate samples of θ.

A priori, we do not know what form the (possibly nonlinear) function f has, and thus we will assume only that it is continuous almost everywhere. Furthermore, from the problem specification (S33), the only constraint on the probability

density P_γ is that it must have zero mean, which is too weak of a constraint to justify using any specific parametric family of distributions. Therefore, we reconstruct both functions in a non-parametric manner. That is, f and P_γ are treated as discrete sets of values to be inferred using MCMC.

Let us denote the discrete ordered list of sample points for the histograms (i.e., bin centers) by

$$\mathbf{x} = [x_1, x_2, \ldots, x_M]$$

and

$$\mathbf{y} = \left[y_1, y_2, \ldots, y_Q\right]$$

such that $\mathbf{P_X} = P\left(X \in [\mathbf{x}, \mathbf{x} + dx]\right)$ and $\mathbf{P_Y} = P\left(Y \in \left[\mathbf{y}, \mathbf{y} + dy\right]\right)$. We aim to choose the parametrization of the function f in order to maximize the robustness of our computational approach. In order to do this, we take into account two intrinsic properties of our optimization problem. First, equation (S32) indicates that it is critical to know the derivative of f at the discrete values $\mathbf{x}$. Therefore, we choose to parametrize f primarily by its derivative rather than its value, which also allows for a straightforward means of constraining f to be a monotonic function as required by (S33). With an initial value f_1 for the function f, we may reconstruct f from its derivative using the fundamental theorem of calculus: $f(x) = f_1 + \int_{x_1}^{x} f'(s)\, ds$. Second, we aim to use the same parametrization for the entire class of monotonic functions, including both monotonically increasing and decreasing functions, that can be distinguished by the sign of $f_M - f_1$. In order to achieve both of these goals, we numerically reconstruct the discrete values of the function f from normalized samples of its derivative $\mathbf{f'}$, defined by $\boldsymbol{\phi} \coloneqq \mathbf{f'}/\left(f_M - f_1\right)$, where imposing $\boldsymbol{\phi} \geq 0$ guarantees monotonicity. Using this parametrization, f can be reconstructed using the formula $\mathbf{f}(\mathbf{x}) \coloneqq \mathbf{f}\left(\mathbf{x}\middle|f_1, f_M, \boldsymbol{\phi}\right) = f_1 + (f_M - f_1)\left[S_{\{1,\ldots,M\}}(\boldsymbol{\phi})\right]$, where

$$S_j(\mathbf{f'}) = \begin{cases} 0 & j = 1 \\ \sum_{i=1}^{j-1} \frac{f_i' + f_{i+1}'}{2}(x_{i+1} - x_i) & \text{otherwise} \end{cases}$$

is a trapezoidal approximation to the cumulative integral of f from x_1 to x_j. Furthermore, we may also compute the probability densities at $\bar{Y} = \mathbf{f}(\mathbf{x})$ using

$$\mathbf{P}_{\bar{\mathbf{Y}}}(\theta) \coloneqq \mathbf{P}\left(\bar{Y} = \mathbf{f}(\mathbf{x})\,|\theta\right) = \hat{\mathbf{P}}_{\bar{\mathbf{X}}}(\mathbf{x}) \oslash \left|\left(f_M - f_1\right)\boldsymbol{\phi}\right|,$$

where $\oslash$ denotes Hadamard division or the element-wise division of two vectors.

Bayesian Inference of the Transformation

In order to asses the validity of a given $(2 + M + Q)$-dimensional set of estimated parameters $\theta = [f_1, f_M, \boldsymbol{\phi}, \mathbf{P}_\gamma]$, we need to compare the discrete set of experimental measurements $\mathbf{P_Y}(\mathbf{y})$ with the estimated $\mathbf{P}\left(Y = \mathbf{f}(x)\,|\theta\right) \coloneqq \left(\mathbf{P}_{\bar{Y}} * \mathbf{P}_\gamma\right)$, a problem that is generally complicated by the fact that $\mathbf{y} \neq \mathbf{f}(\mathbf{x})$. To resolve this issue, we introduce an interpolant, given by

$$\tilde{P}_Y\left(y\,|\theta\right) = \begin{cases} \rho_i + \frac{\rho_{i+1} - \rho_i}{f_{i+1} - f_i}\left(y - f_i\right) & \text{if } \exists\, i : f_i < y \leq f_{i+1} \\ 0 & \text{otherwise} \end{cases},$$

where $\rho = \mathbf{P_Y}\left(\mathbf{f}(\mathbf{x})\,|\theta\right)$, allowing us to create a data-fidelity function for a given θ, given by

$$\Delta P(\theta) = \mathrm{KL}\left(\tilde{P}_Y\left(\mathbf{y}\,|\theta\right)|\mathbf{P_Y}\right).$$

Therefore, to solve problem (S33), we use the Gibbs sampler to sample θ from the posterior

$$\pi\left(\theta\,|\mathbf{P_Y}\right) \propto \mathcal{L}\left(\mathbf{P_Y}|\theta\right) Pr(\theta),$$

where $\mathcal{L}\left(\mathbf{P_Y}|\theta\right) = \exp\left[-\left(\Delta P(\theta) + \lambda BV\left(\mathbf{P}_{\bar{Y}}(\theta)\right)\right)\right]$ and $Pr(\theta)$ are the likelihood and prior densities of θ, respectively. Given the MAP estimate $\hat{\theta} = \left[\hat{f}_1, \hat{\mathbf{f}}', \hat{\mathbf{P}}_\gamma\right]$, we may readily obtain a MAP estimate of $\mathbf{f}$, using the formula

$$\hat{\mathbf{f}} = \mathbf{f}\left(\mathbf{x}\middle|\hat{f}_1, \hat{\mathbf{f}}'\right).$$

SUPPORTING REFERENCES

1. Rishita Changede and Michael Sheetz. "Integrin and cadherin clusters: A robust way to organize adhesions for cell mechanics". In: *BioEssays* 39.1 (2017), e201600123. ISSN: 02659247. DOI: 10.1002/bies.201600123. URL: http://doi.wiley.com/10.1002/bies.201600123.
2. Rishita Changede et al. "Nascent Integrin Adhesions Form on All Matrix Rigidities after Integrin Activation". In: *Developmental Cell* 35.5 (2015), pp. 614–621. ISSN: 15345807. DOI: 10.1016/j.devcel.2015.11.001. URL: http://www.ncbi.nlm.nih.gov/pubmed/26625956%20http://linkinghub.elsevier.com/retrieve/pii/S1534580715007157.
3. Olivier Rossier et al. "Integrins β 1 and β 3 exhibit distinct dynamic nanoscale organizations inside focal adhesions". In: *Nature Cell Biology* 14.10 (2012), pp. 1057–1067. ISSN: 14657392. DOI: 10.1038/ncb2588. URL: http://www.nature.com/articles/ncb2588.
4. Taka A. Tsunoyama et al. "Super-long single-molecule tracking reveals dynamic-anchorage-induced integrin function". In: *Nature Chemical Biology* 14.5 (2018), pp. 497–506. ISSN: 15524469. DOI: 10.1038/s41589-018-0032-5. URL: http://www.nature.com/articles/s41589-018-0032-5.
5. Alice Nicolas and Samuel A. Safran. "Limitation of cell adhesion by the elasticity of the extracellular matrix". In: *Biophysical Journal* 91.1 (2006), pp. 61–73. ISSN: 00063495. DOI: 10.1529/biophysj.105.077115. URL: http://www.ncbi.nlm.nih.gov/pubmed/16581840%20http://www.pubmedcentral.nih.gov/articlerender.fcgi?artid=PMC1479082.
6. Frederic Lagarrigue et al. "A RIAM/lamellipodin-talin-integrin complex forms the tip of sticky fingers that guide cell migration". In: *Nature Communications* 6 (2015), p. 8492. ISSN: 2041-1723. DOI: 10.1038/ncomms9492. URL: http://www.ncbi.nlm.nih.gov/pubmed/26419705%20http://www.pubmedcentral.nih.gov/articlerender.fcgi?artid=PMC4589889%20http://www.nature.com/doifinder/10.1038/ncomms9492.
7. Caroline Cluzel et al. "The mechanisms and dynamics of αvβ3 integrin clustering in living cells". In: *Journal of Cell Biology* 171.2 (2005), pp. 383–392. ISSN: 00219525. DOI: 10.1083/jcb.200503017. URL: http://www.ncbi.nlm.nih.gov/pubmed/16247034%20http://www.pubmedcentral.nih.gov/articlerender.fcgi?artid=PMC2171205.
8. S. E. Le Devedec et al. "The residence time of focal adhesion kinase (FAK) and paxillin at focal adhesions in renal epithelial cells is determined by adhesion size, strength and life cycle status". In: *Journal of Cell Science* 125.19 (2012), pp. 4498–4506. ISSN: 0021-9533. DOI: 10.1242/jcs.104273. arXiv: arXiv:0807.1760v1. URL: http://jcs.biologists.org/cgi/doi/10.1242/jcs.104273.
9. Michelle A Digman et al. "Paxillin dynamics measured during adhesion assembly and disassembly by correlation spectroscopy." In: *Biophysical journal* 94.7 (2008), pp. 2819–31. ISSN: 1542-0086. DOI: 10.1529/biophysj.107.104984. URL: http://www.sciencedirect.com/science/article/pii/S0006349508705332.
10. Haguy Wolfenson et al. "A role for the juxtamembrane cytoplasm in the molecular dynamics of focal adhesions". In: *PLoS ONE* 4.1 (2009), e4304. ISSN: 19326203. DOI: 10.1371/journal.pone.0004304. URL: http://www.ncbi.nlm.nih.gov/pubmed/19172999%20http://www.pubmedcentral.nih.gov/articlerender.fcgi?artid=PMC2627934.
11. Chi Li Chiu et al. "Nanoimaging of focal adhesion dynamics in 3D". In: *PLoS ONE* 9.6 (2014), e99896. ISSN: 19326203. DOI: 10.1371/journal.pone.0099896. URL: http://www.ncbi.nlm.nih.gov/pubmed/24959851%20http://www.pubmedcentral.nih.gov/articlerender.fcgi?artid=PMC4069057.
12. Yvonne Aratyn-Schaus and Margaret L Gardel. "Transient frictional slip between integrin and the ECM in focal adhesions under myosin II tension." In: *Current biology : CB* 20.13 (2010), pp. 1145–53. ISSN: 1879-0445. DOI: 10.1016/j.cub.2010.05.049. URL: http://www.ncbi.nlm.nih.gov/pubmed/20541412%20http://www.pubmedcentral.nih.gov/articlerender.fcgi?artid=PMC2902720.
13. D. P. Felsenfeld, D. Choquet, and M. P. Sheetz. "Ligand binding regulates the directed movement of β1 integrins on fibroblasts". In: *Nature* 383.6599 (1996), pp. 438–440. ISSN: 00280836. DOI: 10.1038/383438a0. URL: http://www.nature.com/doifinder/10.1038/383438a0.
14. Alice C. Chang et al. "Single Molecule Force Measurements in Living Cells Reveal a Minimally Tensioned Integrin State". In: *ACS Nano* 10.12 (2016), pp. 10745–10752. ISSN: 1936-0851. DOI: 10.1021/acsnano.6b03314. URL: http://pubs.acs.org/doi/abs/10.1021/acsnano.6b03314.
15. B. Ph Van Milligen et al. "On the applicability of Fick's law to diffusion in inhomogeneous systems". In: *European Journal of Physics* 26.5 (2005), pp. 913–925. ISSN: 01430807. DOI: 10.1088/0143-0807/26/5/023. URL: http://stacks.iop.org/0143-0807/26/i=5/a=023?key=crossref.18ae1d798b557c850b35a3b3bc9d721c.

16. P. F. Tupper and Xin Yang. “A paradox of state-dependent diffusion and how to resolve it”. In: *Proceedings of the Royal Society A: Mathematical, Physical and Engineering Sciences* 468.2148 (2012), pp. 3864–3881. ISSN: 14712946. DOI: 10.1098/rspa.2012.0259. arXiv: 1204.1590. URL: http://rspa.royalsocietypublishing.org/cgi/doi/10.1098/rspa.2012.0259.

17. R. L. Stratonovich. “Fokker-planck equation with discontinuous coefficients and conditions at the surface of discontinuity”. In: *Soviet Radiophysics* 8.4 (1965), pp. 500–505. ISSN: 00338443. DOI: 10.1007/BF01038325. URL: http://link.springer.com/10.1007/BF01038325.

18. A. Nicolas, B. Geiger, and S. A. Safran. “Cell mechanosensitivity controls the anisotropy of focal adhesions”. In: *Proceedings of the National Academy of Sciences* 101.34 (2004), pp. 12520–12525. ISSN: 0027-8424. DOI: 10.1073/pnas.0403539101. URL: http://www.pnas.org/cgi/doi/10.1073/pnas.0403539101.

19. Colin K Choi et al. “Actin and alpha-actinin orchestrate the assembly and maturation of nascent adhesions in a myosin II motor-independent manner.” In: *Nature cell biology* 10.9 (2008), pp. 1039–50. ISSN: 1465-7392. DOI: 10.1038/ncb1763. URL: http://www.ncbi.nlm.nih.gov/pubmed/19160484%20http://www.pubmedcentral.nih.gov/articlerender.fcgi?artid=PMC2827253.

20. Joseph E. Olberding et al. “The non-equilibrium thermodynamics and kinetics of focal adhesion dynamics”. In: *PLoS ONE* 5.8 (2010). Ed. by Markus J. Buehler, e12043. ISSN: 19326203. DOI: 10.1371/journal.pone.0012043. URL: http://dx.plos.org/10.1371/journal.pone.0012043.

21. Xuan Cao et al. “Multiscale model predicts increasing focal adhesion size with decreasing stiffness in fibrous matrices.” In: *Proceedings of the National Academy of Sciences of the United States of America* 114.23 (2017), E4549–E4555. ISSN: 1091-6490. DOI: 10.1073/pnas.1620486114. URL: http://www.ncbi.nlm.nih.gov/pubmed/28468803%20http://www.pubmedcentral.nih.gov/articlerender.fcgi?artid=PMC5468675.

22. Nir S Gov. “Modeling the size distribution of focal adhesions.” In: *Biophysical journal* 91.8 (2006), pp. 2844–7. ISSN: 0006-3495. DOI: 10.1529/biophysj.106.088484. URL: http://www.ncbi.nlm.nih.gov/pubmed/16861281%20http://www.pubmedcentral.nih.gov/articlerender.fcgi?artid=PMC1578473.

23. Zhenhai Li, Fang Kong, and Cheng Zhu. “A model for cyclic mechanical reinforcement”. In: *Scientific Reports* 6.1 (2016), p. 35954. ISSN: 2045-2322. DOI: 10.1038/srep35954. URL: http://www.nature.com/articles/srep35954.

24. Jing Li and Timothy A. Springer. “Integrin extension enables ultrasensitive regulation by cytoskeletal force”. In: *Proceedings of the National Academy of Sciences* 114.18 (2017), pp. 4685–4690. ISSN: 0027-8424. DOI: 10.1073/pnas.1704171114. URL: http://www.pnas.org/lookup/doi/10.1073/pnas.1704171114.

25. Yuriy V Pereverzev, Eugenia Prezhdo, and Evgeni V Sokurenko. “The two-pathway model of the biological catch-bond as a limit of the allosteric model.” In: *Biophysical journal* 101.8 (2011), pp. 2026–36. ISSN: 1542-0086. DOI: 10.1016/j.bpj.2011.09.005. URL: http://www.ncbi.nlm.nih.gov/pubmed/22004757%20http://www.pubmedcentral.nih.gov/articlerender.fcgi?artid=PMC3192973.

26. Fang Kong et al. “Demonstration of catch bonds between an integrin and its ligand”. In: *Journal of Cell Biology* 185.7 (2009), pp. 1275–84. ISSN: 1540-8140. DOI: 10.1083/jcb.200810002. URL: http://www.ncbi.nlm.nih.gov/pubmed/19564406%20http://www.pubmedcentral.nih.gov/articlerender.fcgi?artid=PMC2712956%20http://jcb.rupress.org/content/185/7/1275.

27. Peter Kloeden. *Numerical solution of stochastic differential equations*. Vol. 47. 1-2. Berlin, Heidelberg: Springer Berlin Heidelberg, 1994, pp. 121–126. ISBN: 978-3-642-08107-1. DOI: 10.1080/17442509408833885. arXiv: arXiv:1011.1669v3. URL: https://www.tandfonline.com/doi/full/10.1080/17442509408833885.

28. Christian L. Vestergaard and Mathieu Génois. “Temporal Gillespie Algorithm: Fast Simulation of Contagion Processes on Time-Varying Networks”. In: *PLoS Computational Biology* 11.10 (2015). Ed. by Marcel Salathé, e1004579. ISSN: 15537358. DOI: 10.1371/journal.pcbi.1004579. arXiv: 1504.01298. URL: https://dx.doi.org/10.1371/journal.pcbi.1004579.

29. C Ballestrem et al. “Marching at the front and dragging behind: differential alphaVbeta3-integrin turnover regulates focal adhesion behavior.” In: *The Journal of cell biology* 155.7 (2001), pp. 1319–32. ISSN: 0021-9525. DOI: 10.1083/jcb.200107107. URL: http://www.ncbi.nlm.nih.gov/pubmed/11756480%20http://www.pubmedcentral.nih.gov/articlerender.fcgi?artid=PMC2199321.

30. Kaixi Tang et al. “Paxillin phosphorylation at serine 273 and its effects on Rac, Rho and adhesion dynamics”. In: *PLoS Computational Biology* 14.7 (2018). Ed. by Anand R. Asthagiri, e1006303. ISSN: 15537358. DOI: 10.1371/journal.pcbi.1006303. URL: https://dx.plos.org/10.1371/journal.pcbi.1006303.

31. Fang Kong et al. “Cyclic Mechanical Reinforcement of Integrin Ligand Interactions”. In: *Molecular Cell* 49.6 (2013), pp. 1060–1068. ISSN: 10972765. DOI: 10.1016/j.molcel.2013.01.015. URL: http://www.ncbi.nlm.nih.gov/pubmed/23416109%20http://www.pubmedcentral.nih.gov/articlerender.fcgi?artid=PMC3615084%20http://linkinghub.elsevier.com/retrieve/pii/S1097276513000488.

32. Elisabetta Ada Cavalcanti-Adam et al. “Cell spreading and focal adhesion dynamics are regulated by spacing of integrin ligands.” In: *Biophysical journal* 92.8 (2007), pp. 2964–74. ISSN: 0006-3495. DOI: 10.1529/biophysj.106.089730. URL: http://www.ncbi.nlm.nih.gov/pubmed/17277192%20http://www.pubmedcentral.nih.gov/articlerender.fcgi?artid=PMC1831685.

33. Mark Schvartzman et al. “Nanolithographic Control of the Spatial Organization of Cellular Adhesion Receptors at the Single-Molecule Level”. In: *Nano Letters* 11.3 (2011), pp. 1306–1312. ISSN: 1530-6984. DOI: 10.1021/nl104378f. URL: http://www.ncbi.nlm.nih.gov/pubmed/21319842%20http://www.pubmedcentral.nih.gov/articlerender.fcgi?artid=PMC3061283%20https://pubs.acs.org/doi/10.1021/nl104378f.

34. Diederik P Kingma and Max Welling. *Auto-Encoding Variational Bayes*. Tech. rep. arXiv: 1312.6114v10. URL: https://arxiv.org/pdf/1312.6114.pdf.

35. Oren Rippel and Ryan Prescott Adams. *High-Dimensional Probability Estimation with Deep Density Models*. Tech. rep. 2013. arXiv: 1302.5125v1. URL: http://math.mit.edu/.

36. Laurent Dinh, Jascha Sohl-Dickstein, and Samy Bengio. “Density estimation using Real NVP”. In: *arXiv* arXiv (2016), p. 1605.08803v3. arXiv: 1605.08803. URL: https://arxiv.org/abs/1605.08803v3.

37. Pooyan Khajehpour Tadavani. *Nonlinear Dimensionality Reduction by Manifold Unfolding*. Tech. rep. URL: https://pdfs.semanticscholar.org/42ab/6c438bf5a6e0e74cc2dd9192a12f2406ca33.pdf.

38. S. Roberts et al. “Gaussian processes for time-series modelling”. In: *Philosophical Transactions of the Royal Society A: Mathematical, Physical and Engineering Sciences* 371.1984 (2012), pp. 20110550–20110550. ISSN: 1364-503X. DOI: 10.1098/rsta.2011.0550. URL: http://rsta.royalsocietypublishing.org/cgi/doi/10.1098/rsta.2011.0550.

39. Trevor Hastie and Robert Tibshirani. “Generalized additive models for medical research”. In: *Statistical Methods in Medical Research* 4.3 (1995), pp. 187–196. ISSN: 0962-2802. DOI: 10.1177/096228029500400302. URL: http://journals.sagepub.com/doi/10.1177/096228029500400302.

40. C E Rasmussen and C K I Williams. *Gaussian Processes for Machine Learning*. 1st ed. MIT Press, 2006, p. 248. ISBN: 026218253X. URL: www.GaussianProcess.org/gpml.

41. Sherjil Ozair and Yoshua Bengio. *Deep Directed Generative Autoencoders*. Tech. rep. arXiv: 1410.0630v1. URL: https://arxiv.org/pdf/1410.0630.pdf.

42. Daniele Perrone and Paolo Favaro. “A Clearer Picture of Total Variation Blind Deconvolution”. In: *IEEE Transactions on Pattern Analysis and Machine Intelligence* 38.6 (2016), pp. 1041–1055. ISSN: 0162-8828. DOI: 10.1109/TPAMI.2015.2477819. URL: http://ieeexplore.ieee.org/document/7254197/.

43. A. N. Tikhonov and Arsenin V. Y. *Solutions of ill-posed problems*. Winston, 1977, p. 258. ISBN: 0470991240.